frontiers in Physics

ORIGINAL RESEARCH
published: 03 January 2022
doi: 10.3389/fphy.2021.809752

Dual-Band Bandpass Filter With Controllable Stopband Bandwidth

*Nan Wang[1], Haokun Wei[1], Kun Gao[2], Xiting Ruan[2], Xiaojian Chen[3], Qian Xu[4], Qian Yang[5], Anxue Zhang[5] and Shuangyang Liu[5]**

[1]State Grid Shaanxi Electric Power Research Institute, Xi'an, China, [2]State Grid Xi'an Electric Power Corporation, Xi'an, China, [3]State Grid Shaanxi Maintenance Company, Xi'an, China, [4]State Grid Weinan Electric Power Corporation, Shangluo, China, [5]School of Information and Communications Engineering, Xi'an Jiaotong University, Xi'an, China

A novel dual-band bandpass filter (BPF) is proposed with independently controllable transmission zeros (TZs) which can realize widely tunable stopband bandwidth (BW). The planar microstrip filter consists of a three-degree L-C ladder lowpass filter loaded with two unsymmetrical shorted stubs which are used to produce different TZs. By tuning the parameters of the two unsymmetrical shorted stubs, the TZs can be independently controlled. Therefore, the BPF has independent controllable center frequencies (CFs), passband bandwidths, and stopband bandwidths between adjacent passbands. All the L-C values in the equivalent circuit of the proposed filter are optimized to fulfill the design specifications. For demonstration, a dual-band BPF is designed. The measured results show good agreement with the simulated ones.

Keywords: bandpass filter, dual-band, tunable stopband, wide upper stopband, transmission zeros, transmission poles

OPEN ACCESS

Edited by:
Zhewang Ma,
Saitama University, Japan

Reviewed by:
Weiren Zhu,
Shanghai Jiao Tong University, China
Yijun Cai,
Xiamen University of Technology, China

****Correspondence:***
Shuangyang Liu
lsy6820@stu.xjtu.edu.cn

Specialty section:
This article was submitted to Optics and Photonics, a section of the journal Frontiers in Physics

Received: *05 November 2021*
Accepted: *29 November 2021*
Published: *03 January 2022*

Citation:
Wang N, Wei H, Gao K, Ruan X, Chen X, Xu Q, Yang Q, Zhang A and Liu S (2022) Dual-Band Bandpass Filter With Controllable Stopband Bandwidth. Front. Phys. 9:809752. doi: 10.3389/fphy.2021.809752

INTRODUCTION

Modern wireless communication systems need high performance filters which have controllable CFs, passband bandwidths, stopband bandwidths, and sharp rejection. Different designing structures and methods have been greatly studied [1–17]. Generally, the dual-band bandpass filter (BPF) adjusts the CFs by changing transmission poles (TPs) [1, 2]. To suppress the harmonic responses, the multiple resonant modes excited by a stepped impedance stub-loaded resonator are used to design dual-band BPFs with a wide upper stopband [3]. However, there is only one transmission zero (TZ) in the stopband. Therefore, the stopband bandwidth is narrow. By introducing more TZs in the stopband, the performances of selectivity and stopband bandwidth can be enhanced. Signal-interference principles [4–6] are applied to design single- or dual-band BPFs with broad stopband bandwidths by creating multiple TZs. To design high performance filters with multiple passbands, the method of multiple mono-frequency resonators coupling to a non-resonating node is proposed in [7]. To have more TZs, couplings between the non-resonating nodes are introduced in [8], or couplings and more open/shorted-subs [9, 10] are applied in the configurations. However, it is difficult to realize the coupling for application when the number of passband increases. Moreover, TZs introduced by the coupling matrix need to change all the coupling coefficients, so it is also difficult to independently adjust the position of TZs [11].

This study presents a novel BPF loaded with two unsymmetrical shorted stubs to introduce two different TZs in the stopband to realize the controllable stopband bandwidth. Following our early work [12], the theoretical analysis of the TZs and TPs is shown in this study, which can demonstrate that the design method has advantages of simplicity and effectiveness. A three-degree lowpass filter

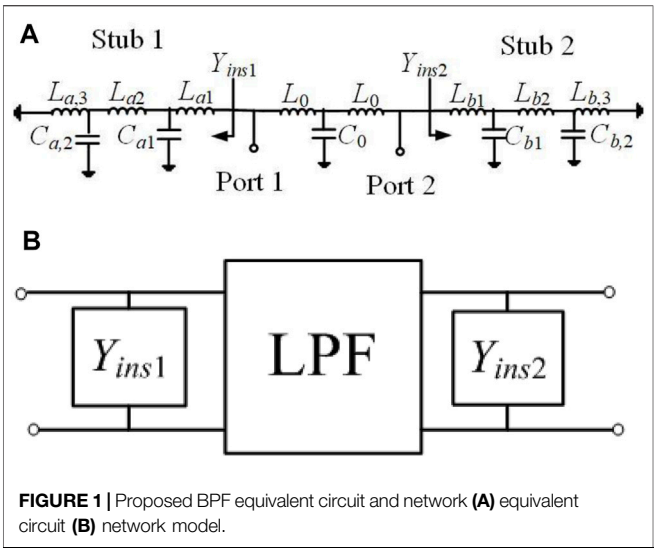

FIGURE 1 | Proposed BPF equivalent circuit and network **(A)** equivalent circuit **(B)** network model.

prototype is chosen for simplicity; the in-band performance will be improved when choosing more degrees of the lowpass filter prototype. A dual-band BPF has been designed and fabricated to verify the proposed concept.

ANALYSIS

The equivalent circuit and network of the proposed prototype are shown in **Figure 1**. The network can be divided into three subnetworks, as shown in **Figure 1B**, which are the lowpass filter (LPF) section in the middle and two unsymmetrical shunt admittance sections at the sides. The LPF section is also a symmetric network and has chosen a three order L-C ladder prototype for simplicity, as shown in **Figure 1A**.

From our early analysis in [12], the shorted stub with two equivalent capacitors will introduce two TZs. As shown in **Figure 1**, the configuration has two unsymmetrical shorted stubs; the shunt admittances of Stub1 and Stub 2 have different LC values, which will produce four different TZs.

The ABCD matrix of the transmission network in **Figure 1B** is expressed as follows, where M_{Y1} and M_{Y2} are the ABCD matrices of the Stub 1 and Stub 2, respectively. M_{LPF} is the ABCD matrix of the middle LPF section. According to the relationship of scattering parameters with the ABCD matrix, the TZs and the reflection zeros (TPs) are the roots of polynomials $P(s)$ and $F(s)$, respectively, where the impedance of the source/load is normalized to be 1. When the root of $F(s)$ is an imaginary number, the reflection zero related to the root represents a TP.

$$M_{Y1} = \begin{bmatrix} 1 & 0 \\ Y_{ins1} & 1 \end{bmatrix} = \begin{bmatrix} 1 & 0 \\ \dfrac{D_1(s)}{N_1(s)} & 1 \end{bmatrix} = \frac{1}{N_1(s)} \begin{bmatrix} N_1(s) & 0 \\ D_1(s) & N_1(s) \end{bmatrix}, \tag{1a}$$

$$N_1(s) = C_{a1}C_{a2}L_{a1}L_{a2}L_{a3}s^5 + [C_{a1}L_{a1}(L_{a2}+L_{a3}) + C_{a2}L_{a3}(L_{a1}+L_{a2})]s^3 + (L_{a1}+L_{a2}+L_{a3})s, \tag{1b}$$

$$D_1(s) = C_{a1}C_{a2}L_{a2}L_{a3}s^4 + (C_{a1}L_{a2} + C_{a1}L_{a3} + C_{a2}L_{a3})s^2 + 1, \tag{1c}$$

$$M_{Y2} = \begin{bmatrix} 1 & 0 \\ Y_{ins2} & 1 \end{bmatrix} = \begin{bmatrix} 1 & 0 \\ \dfrac{D_2(s)}{N_2(s)} & 1 \end{bmatrix} = \frac{1}{N_2(s)} \begin{bmatrix} N_2(s) & 0 \\ D_2(s) & N_2(s) \end{bmatrix}, \tag{2a}$$

$$N_2(s) = C_{b1}C_{b2}L_{b1}L_{b2}L_{b3}s^5 + [C_{b1}L_{b1}(L_{b2}+L_{b3}) + C_{b2}L_{b3}(L_{b1}+L_{b2})]s^3 + (L_{b1}+L_{b2}+L_{b3})s, \tag{2b}$$

$$D_2(s) = C_{b1}C_{b2}L_{b2}L_{b3}s^4 + (C_{b1}L_{b2} + C_{b1}L_{b3} + C_{b2}L_{b3})s^2 + 1, \tag{2c}$$

$$M_{LPF} = \begin{bmatrix} L_0C_0s^2+1 & L_0^2C_0s^3 + 2L_0s \\ C_0s & L_0C_0s^2+1 \end{bmatrix} = \begin{bmatrix} a(s) & b(s) \\ c(s) & d(s) \end{bmatrix}, \tag{3}$$

$$\begin{bmatrix} A & B \\ C & D \end{bmatrix} = M_{Y1} \times M_{LPF} \times M_{Y2} = \frac{1}{N_1(s)N_2(s)} \begin{bmatrix} A'(s) & B'(s) \\ C'(s) & D'(s) \end{bmatrix} = \frac{1}{P(s)} \begin{bmatrix} A'(s) & B'(s) \\ C'(s) & D'(s) \end{bmatrix}, \tag{4a}$$

$$P(s) = N_1(s)N_2(s), \tag{4b}$$

$$F(s) = A'(s) + B'(s) - C'(s) - D'(s) = N_1(s)N_2(s)[b(s) - c(s)] - [N_1(s)D_2(s) + D_1(s)N_2(s)]a(s) - D_1(s)D_2(s)b(s). \tag{5}$$

From (**Eq. 4b**), polynomial $P(s)$ has $4n+2$ roots ($n = 2$), of which 2 roots are at the origin and others are conjugate and symmetrical on the imaginary axis. Therefore, each shorted stub produces n TZs and the two unsymmetrical shorted stubs produce $2n$ different TZs on the imaginary axis. From (**Eq. 5**), the degree of polynomial $F(s)$ is $4n+5$. $N_1(s)$, $N_2(s)$, $b(s)$, and $c(s)$ have odd terms only, while $D_1(s)$, $D_2(s)$, and $a(s)$ have constant terms. Therefore, polynomial $F(s)$ has one root at the origin; two real roots and the remaining $4n+2$ roots are conjugate and symmetrical on the imaginary axis or in four quadrants. The optimization algorithm is used to obtain the required lumped element values for independently controlling the TZs and the return losses, such as genetic algorithm and so on.

Since one of the two shorted stubs can tune two TZs, a dual-band BPF is presented for demonstration. The optimized L-C values are shown in **Table 1**. The S-parameters of the circuit with different parameters of the shorted stub are shown in **Figures 2**, **3**. The parameter L_{a1} of the shorted stub 1 can tune TZ_1 and TZ_4, which means the first passband CF and stopband bandwidth can

TABLE 1 | Optimized L-C values for a dual-band BPF (*L* unit in nH, *C* unit in pF).

L_{a1}	L_{a2}	L_{a3}	L_{b1}	L_{b2}	L_{b3}
0.6923	2.1267	2.2803	0.6053	2.6080	2.0501
C_{a1}	C_{a2}	C_{b1}	C_{b2}	C_0	L_0
0.9256	2.0160	1.4576	1.3815	0.9321	1.7690

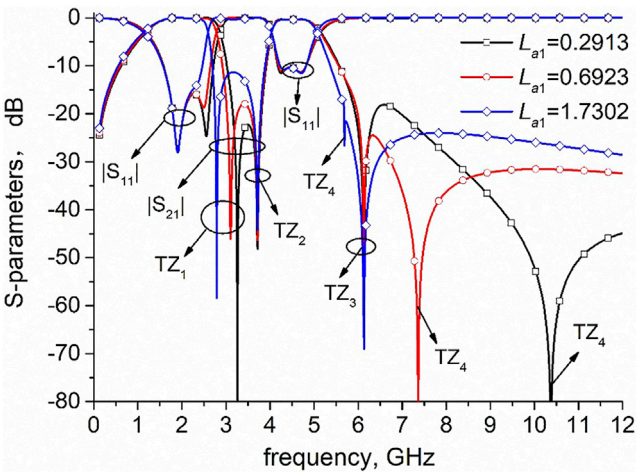

FIGURE 2 | Tunable TZ_1 and TZ_4 versus different L_{a1}.

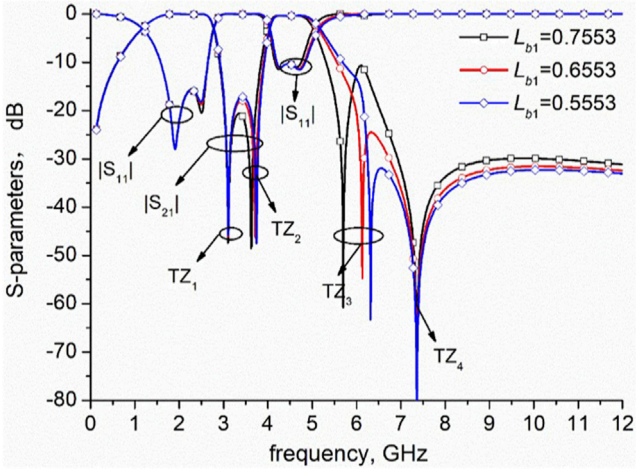

FIGURE 3 | Tunable TZ_2 and TZ_3 versus different L_{b1}.

be tuned independently, while the second passband width, TZ_2 and TZ_3 keep unchanged. The larger the value of L_{a1}, the smaller will be the frequencies of TZ_1 and TZ_4. Meanwhile, when the parameter L_{b1} of the shorted stub 2 changes, the frequencies of TZ_2 and TZ_3 vary simultaneously. As shown in **Figure 3**, the value of L_{b1} gets large and the frequencies of TZ_2 and TZ_3 decrease, which move at the same direction as that of TZ_1 and TZ_4. Therefore, the bandwidth of the second passband can be

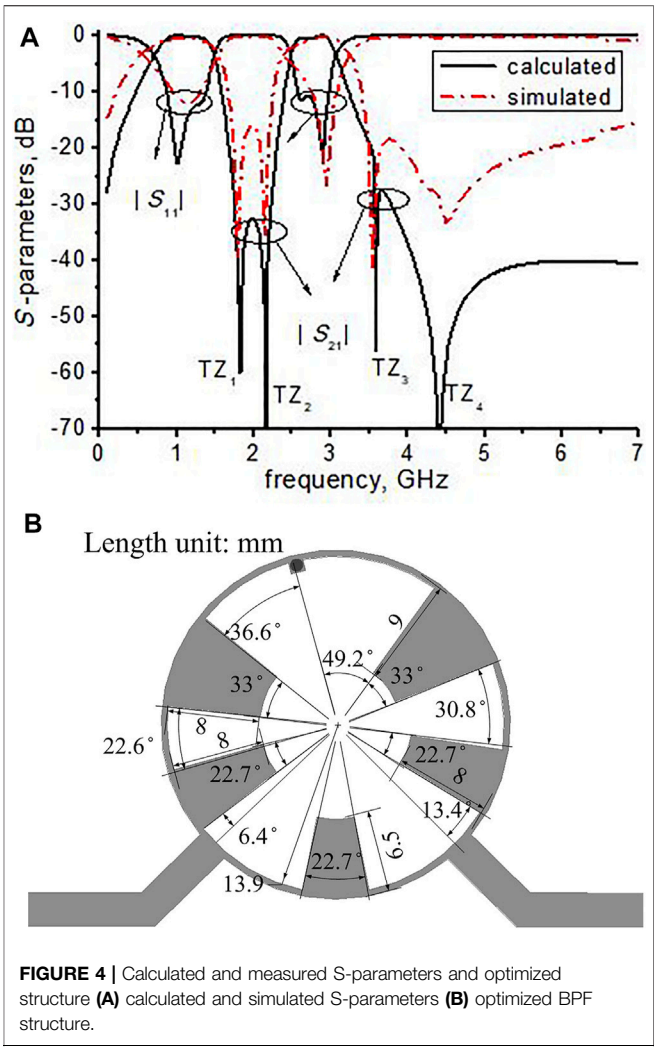

FIGURE 4 | Calculated and measured S-parameters and optimized structure **(A)** calculated and simulated S-parameters **(B)** optimized BPF structure.

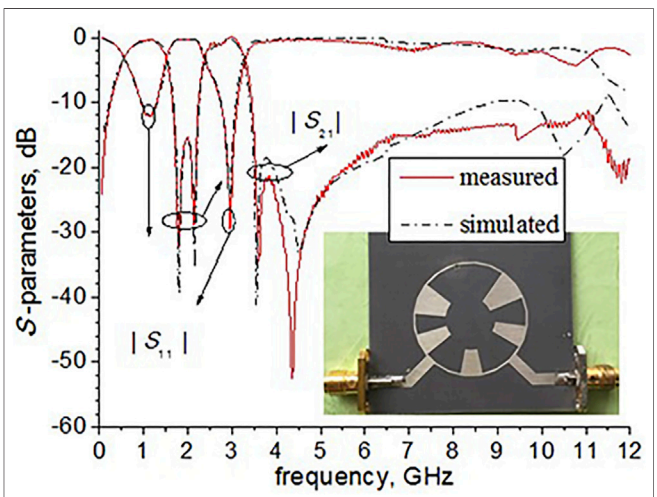

FIGURE 5 | Simulated and measured S-parameters with photograph inset.

TABLE 2 | Comparison of the proposed filter with previous designs.

Ref.	CF (GHz)/FBW (%)	IL (dB)	OBS	Controllable TZs	Size ($\lambda_g \times \lambda_g$)
[3]	1.5/12.7, 2.41/9.1	1.1, 0.9	2.4 f_{02}, >20 dB	--	0.12 × 0.09
Prototype 2 in [4]	0.68/94.9, 2.33/26.4	0.09, 0.83	--	3	0.5 × 0.75
[7]	0.72/16.7, 1/13	0.55, 0.6	--	3	0.27 × 0.39
[8]	0.7/--, 0.8/--	--	1.3 f_{02}, >20 dB	2	--
[12]	1.08/103.2, 3.05/48.5	0.2, 0.6	2.7 f_{02}, >15 dB	2	0.2 × 0.19
This work	1.03/91.3, 2.8/31	0.5, 0.8	4.3 f_{02}, >10 dB	4	0.15 × 0.15

tuned independently. Since the position of the last TP is near that of TZ_3, the upper stopband performance is effected by the move of TZ_3.

RESULTS

A dual-band BPF is designed and fabricated to demonstrate the design method. The CFs of dual passbands are 1 and 2.8 GHz, respectively. The stopbands are 1.75–2.2 GHz (<25 dB) and >3.55 GHz (<25 dB), respectively. Therefore, the TPs are preset as 1.8, 2.15, 3.6, and 4.4 GHz. The optimized L-C values are L_{a1} = 0.5922, L_{a2} = 2.5267, L_{a3} = 3.3803, L_0 = 3.0691, L_{b1} = 1.1153, L_{b2} = 2.4080, L_{b3} = 3.9501 (unit in nH), C_{a1} = 2.8256, C_{a2} = 3.2161, C_0 = 1.4321, C_{b1} = 2.8576, and C_{b2} = 3.6815 (unit in pF). The S-parameters calculated by the optimized L-C values are shown in **Figure 4A**. The roots of $P(s)$ are 0, 0, ±1.83j, ±2.16j, ±3.59j, and ±4.41j, which are calculated in unit GHz for facility. The positive imaginary roots of $P(s)$ represent the TZs. The L-C values of shunt admittance Y_{ins1} control TZ_2 and TZ_4, while the L-C values of shunt admittance Y_{ins2} control TZ_1 and TZ_3. The roots of $F(s)$ are 0, −0.05 ± 1.01j, 0.1 ± 1.37j, −0.07 ± 2.59j, 0.04 ± 2.9j, 0.03 ± 3.58j, −8.94, and 15.15. Since the roots 0.03 ± 3.58j of $F(s)$ are close to the roots ±3.59j of $P(s)$, the second passband has two TPs not three TPs [7].

The BPF is simulated and fabricated on a substrate with ε_r = 2.65, tanδ = 0.003, and h = 1 mm. Here, we choose the 117.8 Ω high-impedance line, which has the line-width of 0.5 mm. As shown in **Figure 4B**, the line width of the open stub which acts as the capacitor is tapered. The characteristic impedance is calculated by the waist width of the taper. Due to the discontinuity of the microstrip line and the minor coupling between the open stubs, the final dimension parameters are optimized by the full-wave electromagnetic simulation software HFSS. The optimized values of parameters are given in **Figure 4B**. The circuit size is about 0.15 λ_g × 0.15 λ_g, where λ_g is the guided wavelength at f_{01}. The simulated S-parameters agree well with the calculated ones, as shown in **Figure 4A**. **Figure 5** shows the simulated and measured S-parameters with the photograph inset. The measured results are in good agreement with the simulated ones. The discrepancies between the simulated results and the measured results may be due to the ignorance of transmission line discontinuity and fabrication tolerances. The measured CFs, fractional bandwidths (FBWs), insertion losses (ILs) at the CF, out-band suppressions (OBSs), the number of controllable TZs, and the size are listed in **Table 2**. As shown in **Table 2**, the proposed dual-band BPF with simple circuit topology has advantages such as relative low IL, wide FBW, wide upper stopband, and more controllable TZs.

CONCLUSION

A dual-band BPF with a controllable stopband bandwidth between the passbands is designed by the method of independently controlling TZs. By tuning the parameters of the two unsymmetrical shorted stubs, the introduced two TZs between adjacent passbands can be independently controlled. After optimizing the equivalent circuit lumped element values, the CFs, passband bandwidths, and stopband bandwidths can be tuned in a certain range. With a simple filter structure and good performance, the proposed method is attractive for application in high-selectivity filter designs.

DATA AVAILABILITY STATEMENT

The original contributions presented in the study are included in the article/Supplementary Material; further inquiries can be directed to the corresponding author.

AUTHOR CONTRIBUTIONS

All authors listed have made a substantial, direct, and intellectual contribution to the work and approved it for publication.

REFERENCES

1. He J, Chen C-m. A Dual-Band BPF with Controllable Center Frequencies and Bandwidths Using a Single SIW Cavity. In: Prceeding of the 2021 IEEE 4th International Conference on Electronics Technology (ICET); 7-10 May 2021; Chengdu, China. IEEE (2021). p. 489–92. doi:10.1109/ICET51757.2021.9451069
2. Lin W, Lee T-H, Wu K Dual-Band Bandpass SIW Resonator Filter with Flexible Frequency Ratio. In: Prceeding of the 2019 49th European Microwave Conference (EuMC); 1-3 Oct. 2019; Paris, France. IEEE (2019). p. 364–7. doi:10.23919/EuMC.2019.8910700

3. Lin L, Sun SJ, Wu B, Liang CH Dual-band Bandpass Filter with Wide Upper Stopband Using Quad-mode Stepped Impedance Stub-loaded Resonator. *Electron Lett* (2014) 50(16):1145–6. doi:10.1049/el.2014.2004
4. Sanchez-Soriano MA, Gomez-Garcia R Sharp-Rejection Wide-Band Dual-Band Bandpass Planar Filters with Broadly-Separated Passbands. *IEEE Microw Wireless Compon Lett* (2015) 25(2):97–9. doi:10.1109/LMWC.2014.2382669
5. Phani Kumar KV, Karthikeyan SS Compact, High Selectivity and Wideband Bandpass Filter with Multiple Transmission Zeros. *AEU - Int J Electronics Commun* (2018) 94:79–83. doi:10.1016/j.aeue.2018.06.047
6. Yogesh SS, Phani K, Karthikeyan SS Compact Dual-Wideband Bandpass Filter for Wireless Applications. *AEU - Int J Electronics Commun* (2018) 95: S1434841118304618. doi:10.1016/j.aeue.2018.08.007
7. Gomez-Garcia R, Guyette AC Reconfigurable Multi-Band Microwave Filters. *IEEE Trans Microwave Theor Techn.* (2015) 63(4):1294–307. doi:10.1109/TMTT.2015.2405066
8. Gómez-García R, Guyette AC, Psychogiou D, Naglich EJ, Peroulis D Quasi-Elliptic Multi-Band Filters with Center-Frequency and Bandwidth Tunability. *IEEE Microwave Wireless Components Lett* (2016) 26(3):192–4. doi:10.1109/LMWC.2016.2526026
9. Xu K-D, Li D, Liu Y High-Selectivity Wideband Bandpass Filter Using Simple Coupled Lines with Multiple Transmission Poles and Zeros. *IEEE Microw Wireless Compon Lett* (2019) 29(2):107–9. doi:10.1109/LMWC.2019.2891203
10. Xu KD, Zhang F, Liu Y, Nie W High Selectivity Seventh-order Wideband Bandpass Filter Using Coupled Lines and Open/shorted Stubs. *Electron Lett* (2018) 54(4):223–5. doi:10.1049/el.2017.4233
11. Tang S-C, Chu P-C, Kuo J-T, Wu L-K Dual-band Bandpass Filter Based on Frequency Transformations with Enhanced Inter-band Isolation. In: Prceeding of the 2020 IEEE Asia-Pacific Microwave Conference (APMC); 8-11 Dec. 2020; Hong Kong, Hong Kong. IEEE (2020). p. 758–60. doi:10.1109/APMC47863.2020.9331380
12. Yang Q, Jiao YC, Zhang Z Dual-wideband BPF with Wide Upper Stopband Using Shorted Stepped-impedance Stub-loaded Lowpass Filter. *Electron Lett* (2016) 52(19):1615–6. doi:10.1049/el.2016.2475
13. Xu J, Wu W, Miao C Compact and Sharp Skirts Microstrip Dual-Mode Dual-Band Bandpass Filter Using a Single Quadruple-Mode Resonator (QMR). *IEEE Trans Microwave Theor Techn.* (2013) 61(3):1104–13. doi:10.1109/tmtt.2013.2238949
14. Sun S-J, Su T, Deng K, Wu B, Liang C-H Compact Microstrip Dual-Band Bandpass Filter Using a Novel Stub-Loaded Quad-Mode Resonator. *IEEE Microw Wireless Compon Lett* (2013) 23(9):465–7. doi:10.1109/LMWC.2013.2274038
15. Peng Y, Zhang L, Fu J, Wang Y, Leng Y Compact Dual-Band Bandpass Filter Using Coupled Lines Multimode Resonator. *IEEE Microw Wireless Compon Lett* (2015) 25(4):235–7. doi:10.1109/LMWC.2015.2400936
16. Jin X, Wen W, Chen M Compact Microstrip Dual-/Tri-/Quad-Band Bandpass Filter Using Open Stubs Loaded Shorted Stepped-Impedance Resonator. *IEEE Trans Microwave Theor Tech* (2013) 61(9):3187–99. doi:10.1109/TMTT.2013.2273759
17. Kim CH, Chang K Independently Controllable Dual-Band Bandpass Filters Using Asymmetric Stepped-Impedance Resonators. *IEEE Trans Microwave Theor Techn.* (2011) 59(12):3037–47. doi:10.1109/TMTT.2011.2168973

Conflict of Interest: Authors NW and HW were employed by the State Grid Shaanxi Electric Power Research Institute. KG and XR were employed by the company State Grid Xi'an Electric Power Corporation. XC was employed by the State Grid Shaanxi Maintenance Company. QX was employed by the State Grid Weinan Electric Power Corporation.

The remaining authors declare that the research was conducted in the absence of any commercial or financial relationships that could be construed as a potential conflict of interest.